ACS APPLIED MATERIALS & INTERFACES

RESEARCH ARTICLE

www.acsami.org

Mesoporous Coaxial Titanium Nitride-Vanadium Nitride Fibers of Core−shell Structures for High-Performance Supercapacitors

Xinhong Zhou,[†] Chaoqun Shang,[†] Lin Gu,[‡] Shanmu Dong,[§] Xiao Chen,[§] Pengxian Han,[§] Lanfeng Li,[†] Jianhua Yao,[§] Zhihong Liu,[§] Hongxia Xu,[§] Yuwei Zhu,[§] and Guanglei Cui*[,§]

[†]Qingdao University of Science and Technology, Qingdao 266042, P. R. China

[§]Qingdao Institute of Bioenergy and Bioprocess Technology, Chinese Academy of Sciences, Qingdao 266101, P. R. China

[‡]Institute of Physics, Chinese Academy of Sciences, Beijing 100080, P. R. China

ABSTRACT: In this study, titanium nitride-vanadium nitride fibers of core−shell structures were prepared by the coaxial electrospinning, and subsequently annealed in the ammonia for supercapacitor applications. These core−shell (TiN-VN) fibers incorporated mesoporous structure into high electronic conducting transition nitride hybrids, which combined higher specific capacitance of VN and better rate capability of TiN. These hybrids exhibited higher specific capacitance (2 mV s^{-1}, 247.5 F g^{-1}) and better rate capability (50 mV s^{-1}, 160.8 F g^{-1}), which promise a good candidate for high-performance supercapacitors. It was also revealed by electrochemical impedance spectroscopy (EIS) and X-ray photoelectron spectroscopy (XPS) characterization that the minor capacitance fade originated from the surface oxidation of VN and TiN.

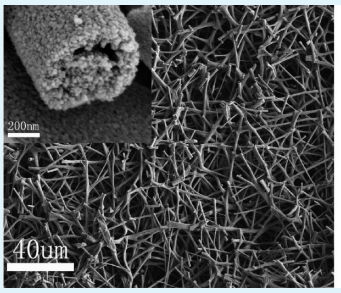

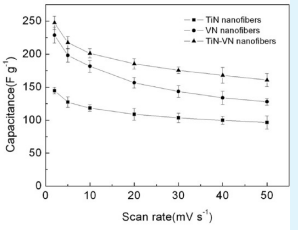

KEYWORDS: titanium nitride-vanadium nitride, fibers, core−shell structures, electrospinning, mesoporous structure, supercapacitor, oxidation

INTRODUCTION

Supercapacitors,[1−5] which are promising power sources for portable devices and automotive applications,[6,7] have many advantages compared to secondary batteries such as simple principle of construction, environmental safety, high rate capability, and long cycle life.[8−11] Among numerous probable materials for supercapacitors, nanostructured materials play an important role because of their excellent characteristics.[12,13] Particular attention is given to fibers with mesoporous structures, as their unique dimensional structure and higher surface-area-to-volume ratio are favorable for enhancing electrode−electrolyte interface and thus providing highly electroactive regions with decreased diffusion lengths.[14,15] Furthermore, mesoporous composite fibers fabricated by coaxial electrospinning[16−20] could combine the characteristic properties of outer and inner materials, which are potential materials for supercapacitors.[21−26]

On the other hand, the transition metal nitrides with low cost, high molar density and superior chemical resistance are desirable candidates for supercapacitors.[27] Among the nitrides, titanium nitride (TiN) exhibits a better electronic conductivity but with low capacity, whereas vanadium nitride (VN) possesses a higher capacity in despite of poor electronic conductivity.[28−30] Accordingly, incorporating VN and TiN into an efficiently fast mixed (electron and ion) transportation nanocomposites can be expected to deliver the ingredients for efficient charge transportion and electrochemical energy storage. To the best of our knowledge, no report exists concerning the exploitation of coaxial TiN and VN core−shell structured mesoporous fibers as electrode materials for supercapacitors.

In this paper, we report the synthesis of coaxial electrospinning TiN and VN core−shell structured mesoporous fibers with the spinneret of two coaxial capillaries for supercapacitors. It is demonstrated that the TiN-VN core−shell structured fibers can be proposed as a promising electrode material for supercapacitors.

EXPERIMENTAL SECTION

Materials. Polyvinylpyrrolidone (PVP) ($M_w \approx 1\,300\,000$, Aldrich), tetrabutyl titanate[$Ti(OBu)_4$] (A.R., Tianjin Kermel Chemical Reagent Co., Ltd., China), isopropyl alcohol (A.R., Tianjin Fuyu Fine Chemical Co., Ltd., China), ethylene glycol (A.R., Tianjin Fuyu Fine Chemical Co., Ltd., China), absolute ethanol (Tianjin Fuyu Fine Chemical Co., Ltd., China), and vanadium(III) acetylacetonate (97%, Aldrich) were used.

Preparation of Electrospinning Solutions. For the preparation of titanium dioxide precursor sol, 0.6 g of PVP powder was dissolved in a mixture of 7 mL of isopropyl alcohol and 1 mL of $Ti(OBu)_4$, and the mixture was stirred for about 12 h at room temperature to form a homogeneous sol. To prepare vanadium pentoxide precursor sol, we dissolved 0.8 g of PVP powder in a mixture of 2 mL of ethylene glycol and 6 mL of absolute ethanol, which was allowed to stir for overnight at room temperature. Subsequently, about 0.3 g of vanadium(III) acetylacetonate was added to the solution; the resultant mixture

Received: May 6, 2011
Accepted: July 5, 2011
Published: July 05, 2011

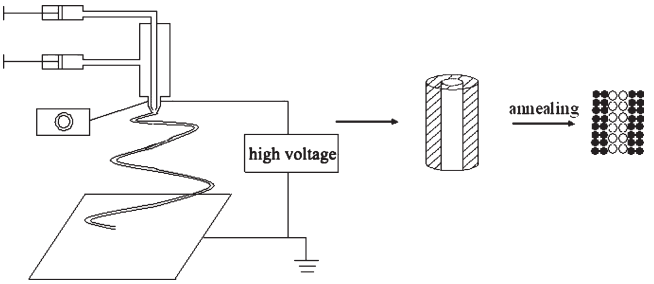

Figure 1. Schematic illustration for the preparation of coaxial TiN-VN core−shell structured mesoporous fibers.[31].

Table 1. Elemental Composition of the TiN Fibers, VN Fibers, and TiN-VN Fibers

materials	Ti%	V%	C%	N%
TiN	69.5 ± 0.2		13.2 ± 0.2	17.3 ± 0.2
VN		68.6 ± 0.2	12.5 ± 0.2	18.8 ± 0.2
TiN-VN	45.8 ± 0.2	24.3 ± 0.2	12.3 ± 0.2	17.6 ± 0.2

was stirred at 80 °C for 20 min and cooled to room temperature naturally.

Fabrication of Core−Shell Structured Fibers. The experimental setup for TiN-VN core−shell structured fibers was illustrated in Figure 1. The core−shell fibers were electrospun by a spinneret which was assembled by two coaxial stainless steel capillaries.[31,32] Typically, the outer and inner diameters of the outer and inner steel capillaries were 1.27 and 0.90 mm, 0.64 and 0.34 mm, respectively. And the inner capillary was 0.5 mm shorter than the outer capillary. The spinneret was connected to the anode of the high-voltage generator, and a piece of aluminum foil was grounded as a collector. The vanadium(III) acetylacetonate sol and $Ti(OBu)_4$ sol were loaded into plastic syringes separately, which were connected to the outer and inner capillaries through polyethylene (PE) tubes and then were pumped out with an individual syringe pump at flow rates of 2.0 and 1.5 mL h^{-1}, respectively. The electrical potential of 23 kV was applied between the capillaries and the ground over a distance of 21.05 cm. For a fair comparison, each kind of fluids was electrospun respectively. The obtained fibers were kept in an oven at 50 °C for 2−4 h to remove the solvents.

Preparation of Mesoporous Core−Shell TiN-VN Fibers. In a typical process, the fibers were heated to 800 °C under ammonia for 1 h with a progressive, slow heating ramp (room temperature to 300 °C, 5 °C min^{-1}; 300 to 700 °C, 2 °C min^{-1}; 700 to 800 °C, 1 °C min^{-1}). After being cooled to room temperature, mesoporous core−shell (TiN-VN) structured fibers were finally obtained as the resultant black powders. For a fair comparison, mesoporous TiN fibers and VN fibers were obtained by the same procedure, respectively.

Characterization. Morphological information was attained from field emission scanning electron microscopy (FESEM, HITACHI S-4800). Selected area electron diffraction (SAED) was performed using a JEOL 4000EX transmission electron microscopy (JEOL, Tokyo, Japan) operated at 400 keV. Elemental analysis was performed using a Flash EA 1112 CHNS/O elemental analyzer from Thermo Scientific. X-ray diffraction (XRD) patterns were recorded with a Bruker-AXS Microdiffractometer (D8 ADVANCE) using Cu Ka radiation (λ = 1.5406 Å) from 30° to 80° at a scanning speed of 0.33° min^{-1}. N_2 adsorption−desorption measurements were carried out at 77 K using a Quantachrome Autosorb gas-sorption system. Brunauer−Emmett−Teller (BET) and Barrett−Joyner−Halenda (BJH) models were used to determine the specific surface areas and the pore sizes of the samples,

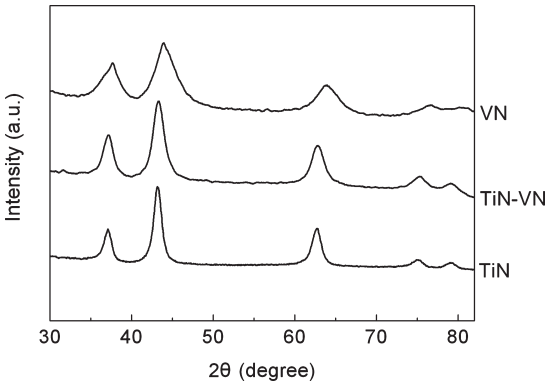

Figure 2. XRD patterns of TiN fibers, VN fibers, and TiN-VN core−shell structured fibers.

respectively. Before the measurements, the samples were degassed at 200 °C under vacuum for at least one night.

Three-electrode system was employed to study the electrochemical performance of the mesoporous TiN-VN fibers. Pt electrode was used as a counter electrode and staturated calomel electrode (SCE) as a reference electrode. The working electrode was prepared by mixing the active nitride materials with 5% conductive carbon blacks (super P) and 10 wt % polytetrafluoroethylene (PTFE) binders. The samples were then cut into plates of 0.5 cm × 0.5 cm and pasted on a stainless steel current-collector (with the thickness of 150 μm) under a pressure of 15 MPa. The electrochemical properties of the electrodes were evaluated by cyclic voltammetry (CV) using a CHI 440A instrument (CHI Instrument Inc.) in 1 M KOH aqueous electrolyte. And electrochemical impedance spectroscopy (EIS) was tested by a ZAHNER ZENNIUM electrochemical workstation (Germany). X-ray photoelectron spectroscopy (XPS) data was obtained with an ESCALab220i-XL electron spectrometer from VG Scientific using Al Ka radiation.

RESULTS AND DISCUSSION

Elemental analysis and inductively coupled plasma (ICP) analysis were applied to investigate elemental composition of the fibers (Table 1). According to elemental analysis, 12.3% carbon can be detected, which showed that the fibers were composited with amorphous carbon.[30,33] XRD patterns of the resultant fibers were displayed in Figure 2, which can be indexed to the typical patterns of crystalline metal nitrides TiN, VN, TiN-VN. No peaks corresponding to titanium oxide or vanadium oxide could be detected in the XRD patterns. Therefore, the presence of large amount of titanium oxide/vanadium oxide can be excluded. The peaks of VN were broadened, indicating a small size of individual crystallites. Compared to pristine TiN and VN fibers, all observed peaks of the nanocomposite did not fit to the positions of VN and TiN. This was indicative of homogeneous TiN-VN structure. In addition, the grain size of TiN-VN fibers was estimated to be approximately 10 nm as calculated from the Scherer equation applied to the (111), (200) and (220) peaks of the TiN-VN. And the lattice parameter calculated from the as-mentioned three peaks was about 4.18 Å. This result was between the TiN typical pattern (JCPDS 38−1420, 4.24 Å) and VN typical pattern (JCPDS 35−0768, 4.14 Å), which also indicated the formation of a solid solution of TiN and VN.[30,34]

Figure 3a depicted that the average outer diameters of the as-prepared fibers amounted about 1020 nm. Subsequently the fibers were subjected to calcination under ammonia, and turned into short fibers with average diameters of 650 ± 20 nm

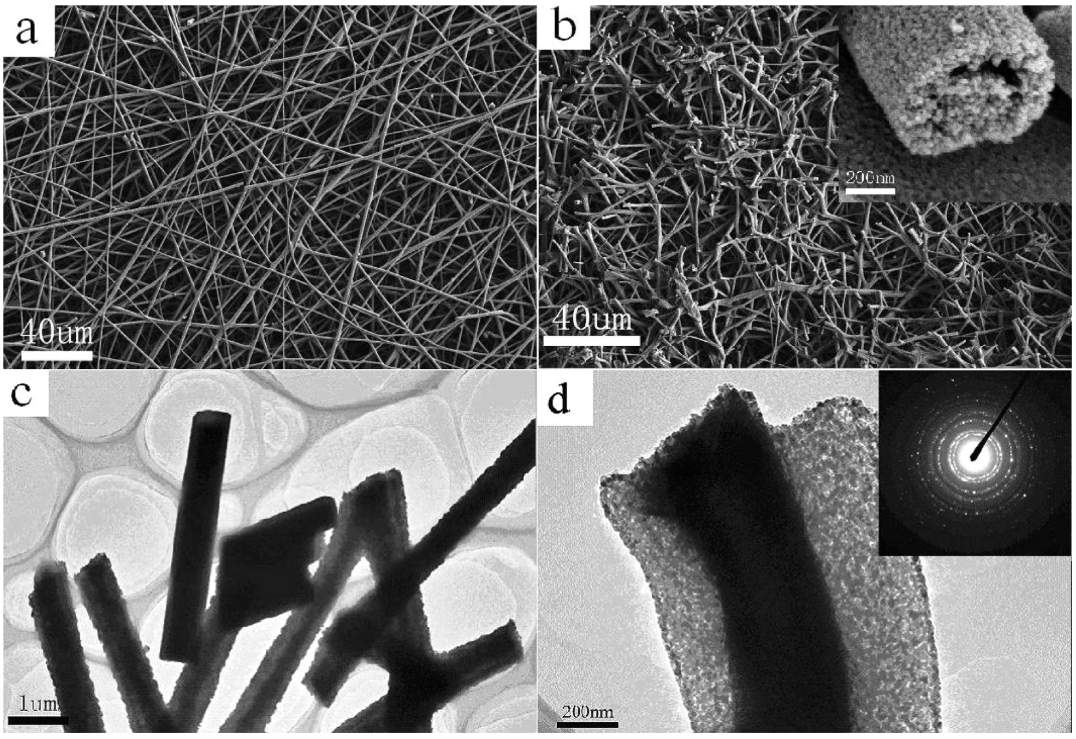

Figure 3. (a) SEM image of preprocessing coaxial fibers. (b) SEM image of TiN-VN fibers. (c) TEM image of TiN-VN fibers. (d) TEM image of the mesoporous TiN-VN fibers.

(Figure 3b) by the removal of the solvents and the carbonization of PVP. The core−shell structure (inset) was clearly observed in the SEM image at high magnification, where inner diameter in the fiber was approximately 300 nm, and the outer diameter of fibers was nearly 660 nm. Figure 3c and 3d exhibited the core−shell structure of TiN-VN with TEM. The fibers were composed of nanoparticles with highly porous structure, which may be accessible to electrolyte and result in a better capacitance characteristic. SAED result (Figure 3d inset) indicated the TiN-VN fibers were polycrystalline.

The porosity of the TiN-VN fibers was determined by nitrogen sorption measurement (Figure 4). The N_2 adsorption−desorption isotherms of all materials were identified as Type IV isotherm indicating characteristics of mesoporous materials. The surface area of TiN-VN fibers was tested to be 169 $m^2\ g^{-1}$, and the average pore size of Barrett−Joyner−Halenda (BJH) was observed to be 3 ± 0.2 nm. All these data strongly confirmed the observation of TEM that the fibers possessed a mesoporous structure. These mesoporous structure might be caused by the pyrolysis and carbonization of PVP, which were beneficial to enhancing specific capacitance.

Cyclic voltammograms (CVs) tests were performed to evaluate its capacitance property. The specific capacitance of supercapacitor (C) was calculated according to the equation[35]

$$C = \frac{\int (Id\varphi)}{2mv\Delta V} \quad (1)$$

where m was the mass of the electrode, and I, v, ΔV, φ are the average current of charge and discharge, scan rate, potential difference and potential range, respectively. Figure 5a showed the CV curves of TiN, VN, and TiN-VN at the scan rate of 20 mV s^{-1}. The capacitance of the TiN-VN fibers was calculated to be 185 F g^{-1}, which was obviously higher than that of TiN fibers (109 F g^{-1}) and VN fibers (157 F g^{-1}). This phenomenon was mainly related to the special structures of TiN-VN fibers. To further quantify their rate performance, we conducted CV studies at different scanning rates. Figure 5b demonstrates the CV curves of the TiN-VN fiber electrode at scan rates of 2, 5, 10, 20, 30, 40, and 50 mV s^{-1}, and the corresponding capacitances were 247.5, 217.5, 201.4, 185.4, 175.6, 168.0, and 160.8 F g^{-1}, respectively. The overall specific capacitance of TiN fibers and VN fibers were also tested for comparison (Figure 5c). The capacitance of TiN fibers was 145, 127, 118, 109, 104, 100, and 97 F g^{-1} at the corresponding scan rates, whereas the capacitance of VN fibers was 229, 198, 182, 157, 143, 134, and 128 F g^{-1}, correspondingly. It was obviously to observe that the TiN fibers electrode had the lowest capacitance but with better capacitance retention at higher scan rate, VN fibers electrode exhibited larger capacitance but worse rate capability. The capacitance of VN in this paper was much lower than the huge value (2 mV s^{-1}, 1340 F g^{-1}) of Choi et al.,[36] but it was in a good agreement with the values (30 mV s^{-1}, 161 F g^{-1}; 5 mV s^{-1}, 221 F g^{-1}) reported by other groups.[37,38] Interestingly, TiN-VN fibers electrode represented a synergetic effect that they exhibited much higher capacitance than TiN fibers electrode, better rate capability than VN fibers electrode. Galvanostatic charge−discharge experiments were further carried out to test the TiN-VN of core−shell structured fibers electrode. The specific capacitance of the TiN-VN measured from galvanostatic charge−discharge tests can be calculated by the equation[39]

$$C = \frac{I\Delta t}{m\Delta V} \quad (2)$$

The galvanostatic charge−discharge curves of TiN-VN fibers at different current densities were shown in Figure 5d. And the

capacitance of the TiN-VN fibers was calculated to be 262 F g^{-1} at the current density of 2 A g^{-1}, and retained 168 F g^{-1}at 10 A g^{-1}.

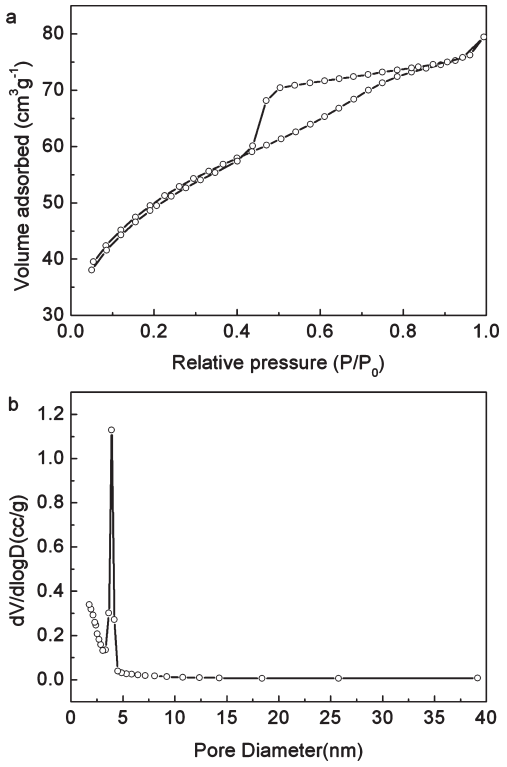

Figure 4. (a) Nitrogen adsorption and desorption isotherms of TiN-VN core−shell structured fibers and (b) their pore-size distribution obtained from adsorption branch of the isotherm using the BJH method.

This result was a little higher than that value obtained by the CV tests, which was in agreement with a previous work.[40]

Correlating the nanostructure and electrochemical performance of the composite, our results were explained as follows. The improvement in its performance was mainly due to the core−shell structure, which integrated together better electrical conductivity of TiN and higher capacitance of VN. The fibers were full of mesoporous pores and nanoscale particles that were beneficial for accessible diffusion of electrolyte. The amorphous carbon nanowiring was also desirable for further improving the rate capability. Consequently, the electrochemical performance of the TiN-VN electrode was improved as a result from the significant enhancement rooting in a mixed transportation nanostructured network, which was partly corroborated by above microscopic characterization.

The electrochemical stability of TiN-VN fiber electrode at the scan rate of 100 mV s^{-1} was depicted in Figure 6. It was

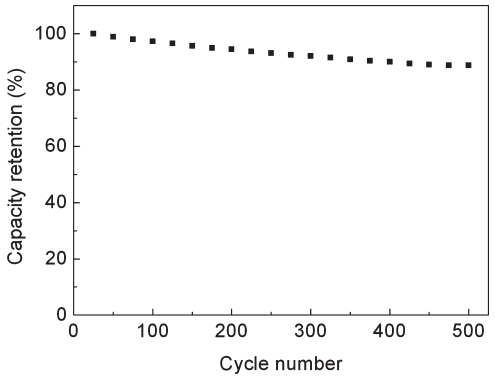

Figure 6. Cycling performance of composite core−shell structured TiN-VN fibers under a scan rate of 100 mV s^{-1}.

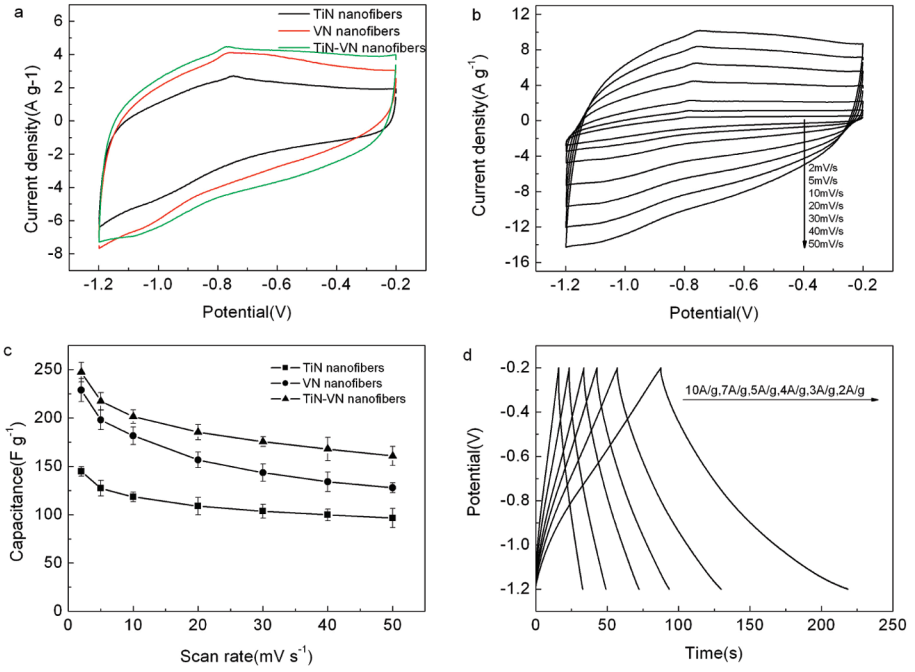

Figure 5. (a) CV curve of TiN, VN, TiN-VN fibers cycled between −1.2 V and −0.2 V at a sweep rate of 20 mV s^{-1}. (b) CV curves of TiN-VN fibers at various potential scanning rates from 2 mV s^{-1} to 50 mV s^{-1}. (c) Specific capacitances of the electrodes with TiN, VN, TiN-VN fibers respectively at progressive scan rates from 2 mV s^{-1} to 50 mV s^{-1}. (d) The charge/discharge curves of TiN-VN fibers between voltage limits of −1.2 to −0.2 V at rates varied from 2 A g^{-1} to 10 A g^{-1}.

dx.doi.org/10.1021/am200564b |ACS Appl. Mater. Interfaces 2011, 3, 3058–3063

seen that about 88% of original capacitance was retained after 500 cycles, exhibiting acceptable cycle ability for the TiN-VN fibers.

Furthermore, EIS was used to study the resistance changes after cycling. Figure 7 represented the variation of electrochemical impedance spectra for TiN-VN fibers before and after 500 cycles, applying 5 mV ac voltage in the frequency range from 0.1 Hz to 100 kHz. Each curve presented a depressed semicircle in middle and high frequency region. At lower frequencies, the straight line had finite slope about 1.3 before cycling and near 1 after cycling, which represented the diffusive behavior changes of electrolyte in the electrode pores. The semicircle in the high-frequency range was associated with the surface properties of the TiN-VN electrode and corresponded to the charge-transfer resistance. An equivalent circuit (inset of Figure 7) was used to analyze the measured impedance data,[41] where R_s was the internal resistance, Q_1 and Q_2 were the double-layer capacitance and pseudocapacitance, respectively,

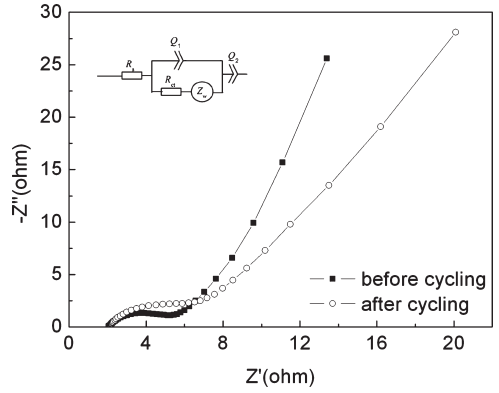

Figure 7. Nyquist plots for TiN-VN fibers electrode before and after 500 cycles from 0.1 Hz to 100 kHz.

R_{ct} was the charge-transfer resistance, and Z_w was the Warburg impedance. An obvious difference between the two spectra was that R_{ct} had increased from 1.68 to 2.52 Ω after 500 cycles, which was probably attributed to the partial oxidation of active nitride materials.[36,37]

To further explain the capacitance fade after cycling, XPS was used to assess the surface of TiN-VN fibers. The binding energies between 513 and 540 eV corresponded to the presence of O 1s, V $2p^1$, and V $2p^3$ peaks. The reported binding energies for V^{3+}, V^{4+} and V^{5+} species were three Gaussian distributions centered at 515.6, 516.5, and 517.3 eV, respectively, with the statistical deviation W_{BE} = 0.25 eV.[42] The XPS spectrum of the surface of TiN-VN fibers was exhibited in Figure 8. After cycling, the peaks of oxygen, titanium and vanadium were obviously increased. In Figure 8a, the enhanced O 1s line after cycling indicated that a thin oxide layer exhibited on the surface of VN and TiN, which was fitted with three peaks. The peaks at about 531.0 and 529.5 eV were main components typical for oxygen in vanadium oxide and titanium oxide.[37] The other peak at 532.7 eV belonged to the signal from −OH groups at the surface of TiN-VN fibers. For the V $2p^3$ line, it was fitted with three peaks at 515.6, 516.6, and 517.3 eV, corresponding to oxidation states of vanadium in surface oxides. It was reported that the Ti 2p bands yields in each case three major doublets ($2p^3$ and $2p^1$) encompassed the set of three $2p^3$ peaks, namely, at 455.1 eV typical for TiN, at 456.7 eV in the range for TiO or TiO_xN_y, and at 458.2 eV for TiO_2.[43,44] As displayed in Figure 8b, after cycling, the strongest Ti $2p^3$ peak at 458.3 eV was found, which reasonably ascribed to TiO_2. Ti $2p^3$ peak at 456.5 eV was for TiN, and the peak at 457.7 eV was typical for TiO or TiO_xN_y. The partial oxidation can make the active nitride material gradually disconnect with current collector, which were corrugated by EIS data and consistent with the previous reports.[36,37] Therefore, it was confirmed that the capacity fade of active TiN-VN was originated from the oxidation of VN and TiN.

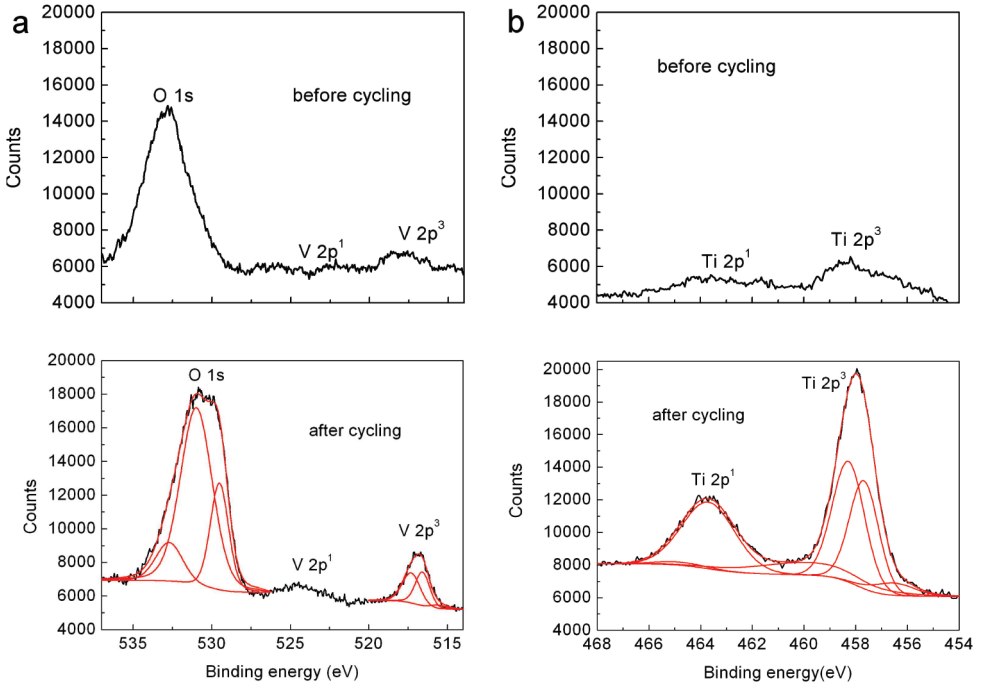

Figure 8. XPS spectra and curve fitting of (a) O 1s, V $2p^3$ and (b) Ti $2p^1$, Ti $2p^3$ spectra of TiN-VN fibers before and after 500 cycles.

CONCLUSION

In summary, we have synthesized the mesoporous TiN-VN fibers with core−shell structures through coaxial electrospinning and subsequent ammonia annealing. It was demonstrated that the nanostructured TiN-VN can combine the advantages of TiN and VN material, which present not only a higher specific capacitance but a better rate capacity than pristine nitride fibers. Our results indicated that this mesoporous nanostructured fiber was a good candidate for high-performance supercapacitors. Furthermore, these coaxial materials could have potential in lithium-ion batteries or electrocatalysts.

AUTHOR INFORMATION

Corresponding Author

*Tel: (+86) 532-80662746. Fax: (+86) 532-80662744. E-mail: cuigl@qibebt.ac.cn.

ACKNOWLEDGMENT

We appreciate the support of "100 Talents" program of the Chinese Academy of Sciences, National Program on Key Basic Research Project of China (973 Program) (MOST2011CB935700), Shandong Province Fund for Distinguished Young Scientist (BS2009NJ013), and National Natural Science Foundation of China (Grants 20971077, 20901044, 20802039, and 20902052).

REFERENCES

(1) Mayer, S. T.; Pekala, R. W.; Kaschmitter, J. L. *J. Electrochem. Soc.* **1993**, *140*, 446.
(2) Yoshida, A.; Nonaka, S.; Aoki, I.; Nishino, A. *J. Power Sources* **1996**, *60*, 213.
(3) Burke, A. *J. Power Sources* **2000**, *91*, 37.
(4) Arico, A. S.; Bruce, P.; Scrosati, B.; Tarascon, J. M.; Schalkwijk, W. V. *Nat. Mater.* **2005**, *4*, 366.
(5) Kibi, Y.; Saito, T.; Kurata, M.; Tabuchi, J.; Ochi, A. *J. Power Sources* **1996**, *60*, 225.
(6) Miller, J. R.; Burke, A. F. *Electrochem. Soc. Interface* **2008**, *17*, 53.
(7) Miller, J. R.; Simon, P. *Science* **2008**, *321*, 651.
(8) An, K. H.; Kim, W. S.; Park, Y. S.; Moon, J. M.; Bae, D. J.; Lim, S. C. *Adv Funct. Mater.* **2001**, *11*, 387.
(9) Probstle, H.; Wiener, M.; Fricke, J. *J. Porous Mater.* **2003**, *10*, 213.
(10) An, K. H.; Kim, W. S.; Park, Y. S.; Choi, Y. C.; Lee, S. M.; Chung, D. C. *Adv. Mater.* **2001**, *13*, 497.
(11) Beguin, F.; Szostak, K.; Lota, G.; Frackowiak, E. *Adv. Mater.* **2005**, *17*, 2380.
(12) Qu, D. Y. *J. Power Sources* **2002**, *109*, 403.
(13) Qu, D. Y.; Shi, H. *J. Power Sources* **1998**, *74*, 99.
(14) Lee, S. I.; Mitani, S.; Park, C. W.; Yoon, S. H.; Korai, Y.; Mochida, I. *J. Power Sources* **2005**, *139*, 379.
(15) Guo, Y. G.; Hu, Y. S.; Maier, J. *Chem. Commun.* **2006**, *26*, 2783.
(16) Lu, X.; Wang, C.; Wei, Y. *Small* **2009**, *5*, 2349.
(17) Theron, S. A.; Yarin, A. L.; Zussman, E.; Kroll, E. *Polymer* **2006**, *46*, 2889.
(18) Reneker, D. H.; Yarin, A. L.; Fong, H.; Koombhongse, S. *J. Appl. Phys.* **2000**, *87*, 4531.
(19) Shin, Y. M.; Hohman, M. M.; Brenner, M. P.; Rutledge, G. C. *Appl. Phys. Lett.* **2001**, *78*, 1149.
(20) Theron, S. A.; Zussman, E.; Yarin, A. L. *Polymer* **2004**, *45*, 2017.
(21) Yu, J. H.; Fridrikh, S. V.; Rutledge, G. C. *Adv. Mater.* **2004**, *16*, 1562.
(22) Bazilevsky, A. V.; Yarin, A. L.; Megarids, C. M. *Langmuir* **2007**, *23*, 2311.
(23) McCann, J. T.; Marquaz, M.; Xia, Y. *Nano Lett.* **2006**, *6*, 2868.
(24) Sun, Z.; Zussman, E.; Yarin, A. L.; Wendorff, J. H.; Greiner, A. *Adv. Mater.* **2003**, *15*, 1929.
(25) Kalra, V.; Mendez, S.; Lee, J. H.; Nguyen, H.; Marquez, M.; Joo, Y. L. *Adv. Mater.* **2006**, *18*, 3299.
(26) Hertz, H.; Hermanrnud, B. *J. Fluid Mech.* **1983**, *131*, 271.
(27) Cabana, J.; Ionica-Bousquet, C. M.; Grey, C. P.; Palacin, M. R. *Electrochem. Commun.* **2010**, *12*, 315.
(28) Choi, D.; Kumta, P. N. *Electrochem. Solid-State Lett.* **2005**, *8*, A418.
(29) Bang, J. H.; Suslick, K. S. *Adv. Mater.* **2009**, *21*, 3186.
(30) Cui, G. L.; Gu, L.; Thomas, A.; Fu, L. J.; Aken, P.; Antonietti, M.; Maier, J. *Chem. Phys. Chem.* **2010**, *11*, 3219.
(31) Chen, H. Y.; Wang, N.; Di, J. C.; Zhao, Y.; Song, Y. L.; Jiang, L. *Langmuir* **2010**, *26*, 11291.
(32) Zhao, Y.; Jiang, L. *Adv. Mater.* **2009**, *21*, 3621.
(33) Ji, L. W.; Zhang, X. W. *Electrochem. Commun.* **2009**, *11*, 795.
(34) Helmersson, H.; Todorova, S.; Barnett, S. A.; Sundgren, J. E.; Markert, L. C.; Greene, J. E. *J. Appl. Phys.* **1987**, *62*, 481.
(35) Chen, W.; Fan, Z. L.; Gu, L.; Bao, X. H.; Wang, C. L. *Chem. Commun.* **2010**, *46*, 3905.
(36) Choi, D.; Blomgren, G. E.; Kumta, P. N. *Adv. Mater.* **2006**, *18*, 1178.
(37) Glushenkov, A. M.; Jurcakova, D. H.; Llewellyn, D.; Lu, G. Q.; Chen, Y. *Chem. Mater.* **2010**, *22*, 914.
(38) Zhou, X. P.; Chen, H. Y.; Shu, D.; He, C.; Nan, J. M. *J. Phys. Chem. Sol.* **2009**, *70*, 495.
(39) Dong, S. M.; Chen, X.; Gu, L.; Zhou, X. H.; Xu, H. X.; Wang, H. B.; Liu, Z. H.; Han, P. X.; Yao, J. H.; Wang, L.; Cui, G. L.; Chen, L. Q. *ACS Appl. Mater. Interfaces* **2011**, *3*, 93.
(40) Pang, S. C.; Anderson, M. A.; Chapmanb, T. W. *J. Electrochem. Soc.* **2000**, *147*, 444.
(41) Xu, C. J.; Du, H. D.; Li, B. H.; Kang, F. Y.; Zeng, Y. Q. *J. Electrochem. Soc.* **2009**, *156*, A73.
(42) Bondarenka, V.; Grebinskij, S.; Mickevicius, S.; Tvardauskas, H.; Kaciulis, S.; Volkov, V.; Zakharova, G.; Pasiskevicius, A. *Lithuanian J. Phys.* **2007**, *47*, 333.
(43) Zukalova, M.; Prochazka, J.; Bastl, Z.; Duchoslav, J.; Rubacek, L.; Havlicek, D.; Kavan, L. *Chem. Mater.* **2010**, *22*, 4045.
(44) Drygas, M.; Czosnek, C.; Paine, R. T.; Janik, J. F. *Chem. Mater.* **2006**, *18*, 3122.